Annular reactor testing and Raman surface characterization in the CPO of methane and propylene

A. Donazzi [a], D. Pagani [a], A. Lucotti [b], M. Tommasini [b], A. Beretta [a], G. Groppi [a,*], C. Castiglioni [b], P. Forzatti [a]

[a] *Politecnico di Milano, Dipartimento di Energia, Piazza Leonardo da Vinci 32, 20133 Milano, Italy*
[b] *Politecnico di Milano, Dipartimento di Chimica Materiali e Ingegneria Chimica, Piazza Leonardo da Vinci 32, 20133 Milano, Italy*

Received 15 March 2013
Received in revised form 21 May 2013
Accepted 4 June 2013
Available online 13 June 2013

1. Introduction

Thanks to the wide availability and to the easy storage and transportation, the use of liquid fuels in short contact time catalytic partial oxidation (CPO) reformers represents a significant advance in on-board and small-scale power generation technologies. The extensive exploitation of LPG and higher hydrocarbons in CPO reformers is currently hampered by the high temperatures reached on the catalyst surface (>1000 °C) and by the formation of carbon species, which lead the catalyst to deactivation by sintering and coking. Both these issues become increasingly crucial upon increasing the complexity and the C number of the fuel. On one hand, in order to moderate the overheating, solutions based on the optimization of the reactor design have been proposed, which concern the geometry of the catalyst support and the layout of the internal elements of the reactor [1,2]. On the other hand, with respect to the issue of carbon formation, given its kinetic nature, possible solutions necessarily ask for a detailed understanding of the process chemistries involved, both homogenous and heterogeneous, and of their possible interplay. Several works dedicated to CPO and autothermal reforming (ATR) of C_3 and higher alkanes [3–16] report non-negligible selectivity to olefins (mainly ethylene and propylene) and cracking products (methane and ethane) at the exit of the reactor, even when noble metals are employed. Olefins in particular are well known coke-precursors: their presence can be taken as an indicator of the possible occurrence of condensation reactions, which lead to the formation of aromatic compounds and later to the growth of carbonaceous layers on the catalyst surface. As a matter of fact, the experimental results generally suggest that olefins are produced by homogenous pyrolysis routes, which activate in parallel to the mainstream heterogeneous routes giving synthesis gas via reforming.

With respect to Rh-based catalysts applied in CPO, the literature concerning higher alkanes has developed to a much smaller

* Corresponding author. Tel.: +39 02 23993258.
E-mail address: gianpiero.groppi@polimi.it (G. Groppi).

extent than that dedicated to CH_4. The reason likely lays in that stable operation is commonly experienced in CH_4 oxy-reformers that work under autothermal conditions [17]. Wide agreement is found upon the evidence that CH_4 is not prone to coking on Rh: CH_4 is indeed regarded as difficult to activate on noble metals, thanks to its low tendency to stick on the surface and to its stronger C—H bond energy compared to larger alkanes [18,19]. When observed [20,21], C formation has been reported as a structure-sensitive process, therefore sensitive to the state of the surface in terms of defects and particle size, and also dependent on the network of reaction steps involved, namely upon the breaking of C—H or C—O bonds or the adsorption of gas-phase intermediates.

In the case of higher alkanes, the group of Schmidt [6,15] reported that Rh-coated alumina foams are able to steadily reform up to C_{16} paraffins, under autothermal conditions, at short contact times and temperature ranging from 800 to 1100 °C, with no deactivation due to coke formation. Such a remarkable resistance was achieved using very high Rh loading with extremely low particle dispersion (almost a film in some cases). The experiments showed that the selectivity to olefins decreased in favor of synthesis gas when a γ-Al_2O_3 washcoat was applied, i.e. when the metal area active for heterogeneous reforming increased. As well, a lower production of olefins was observed by increase of the foam ppi (from 45 to 800 ppi), that is when the pore size decreased and less empty volume was given to homogenous chemistry to evolve.

The onset of coke formation at a certain position of the catalytic monolith was shown numerically and experimentally by the group of Deutschmann in the CPO of i-octane over Rh-based catalysts supported over cordierite honeycombs [8]. A transition point was individuated between a coke-free region, roughly corresponding to the oxygen consumption zone of the catalyst, and a coke-forming region, associated to the zone where the catalyst experiences gas-phase pyrolysis in parallel to surface steam reforming. The position of this coke transition point was found to be very sensitive to the C/O ratio and to the flow rate: it moves upstream with increasing C/O or decreasing flow rate. Consistently, already at C/O = 1.1 (O_2/C = 0.45), a breakthrough of olefins (propylene and i-butylene) and other cracking products was observed. Along with the role of olefins in the CPO of higher alkanes, our group has recently applied spatially resolved profiles of temperature and composition in the autothermal CPO of C_3H_8 over 2 wt% Rh/α-Al_2O_3 catalysts supported over ceramic honeycombs [22]. The results showed that small amounts of methane, ethane, ethylene and propylene are present at the very inlet of the catalyst, in close correspondence of the hot spot. The formation of these species was attributed to homogenous cracking reactions, followed by consumption via steam reforming on the catalyst surface.

Overall, these results suggest that C_{2+} and other intermediate olefins may have a significant impact in the oxy-reforming process, especially when non stoichiometric C/O ratios are used. It is indeed expected that the behavior of olefins is more sensitive to C formation, given that the presence of the C=C double bond increases the affinity with the surface. By application of vibrational spectroscopy techniques under ultrahigh vacuum conditions, Somorjai and co-workers [23] analyzed the reactions of thermal decomposition of propylene, propadiene and methylacetylene on Rh(1 1 1) model surfaces, from 80 to 800 K. Friend and co-workers [24,25] extended this analysis by performing theoretical and experimental studies on the partial oxidation of ethylene and propylene. Globally, the results confirm that the C=C double bond is the active functional group of the olefin and that its activation prevails over that of the allylic C—H bond. On Rh clean surfaces, a dehydrogenation pathway leads via CH_x intermediates to the formation of adsorbed C, which polymerizes to graphitic structures upon increasing the temperature. In the presence of chemisorbed oxygen, partial and total oxidation routes compete favorably with dehydrogenation, being this competition dependent on the oxygen surface coverage.

In order to investigate the role of olefins in the CPO mechanism, in this work we analyze the CPO of C_3H_6 (representative C_{2+} coke-forming fuel) and CH_4 (assumed as the reference coke-free fuel in CPO) performed on Rh-based catalyst, focusing the attention on the tendency to coke formation. The formation of carbon species as a function of temperature and reaction conditions is followed by combining kinetic investigation performed in an annular micro-reactor, with Raman measurements of the catalyst surface. A companion paper will be presented concerning the kinetic effects observed in the C_3H_6 CPO experiments performed in the annular microreactor. Herein, these effects are briefly recalled in the section of results and discussion.

2. Materials and methods

2.1. Catalyst preparation

A 2 wt% Rh/α-Al_2O_3 catalyst was prepared by dry impregnation of the α-Al_2O_3 support (10 m^2/g surface area by BET measurement) with a commercial $Rh(NO_3)_3$ aqueous solution. The impregnated powders were dried in oven at 110 °C for 3 h. For testing in the annular reactor, the catalyst was deposited in the form of thin layers on sintered alumina tubular supports. A dip coating technique was applied, starting from a slurry of the catalyst powders prepared according to a standard recipe [26]. The coated tubular supports were then flash-dried in oven at 280 °C for 10 min to fix the catalyst layer on the external surface of the support. Well adherent layers were obtained, 20 mm long, between 7 and 12 mg in weight and 15–25 μm thick.

2.2. Annular reactor testing

The CPO experiments were performed in an annular reactor. The reactor was externally heated by a tubular furnace and a MicroGC (3000A by Agilent Technologies) was used to analyze the composition of the inlet and outlet gas streams. Detailed descriptions of the reactor and of the set-up are given elsewhere [27]. Here it is worthy to recall that the annular reactor consists of an inner catalyst-coated ceramic tube (O.D. = 4 mm) coaxially inserted into an outer quartz tube (I.D. = 5 mm), giving rise to an annular duct wherein the gas flows in laminar regime. The laminar regime allows to reach very high gas velocity. In this way, it is possible to test fast and exothermic reactions, like the CPO of light hydrocarbons, far from the thermodynamic limitations, in a wide kinetically informative experimental field. Dilution of the reacting mixture and efficient heat dissipation by radiation allow to reach quasi-isothermal conditions on the catalyst layer. At any time, the temperature profile can be verified by sliding a thermocouple inside the tubular ceramic support, given that thermal equilibrium establishes in the cross section of the reactor.

The CPO experiments were carried out at atmospheric pressure between 200 and 850 °C, increasing the temperature by step-wise increments of 10–50 °C. At each temperature, the conversion of the reactants and the molar fraction of the products were estimated by repeated analyses, showing stable performances within 15–20 min. Prior to the kinetic tests, the catalyst underwent a conditioning procedure that consisted of repeated runs at 8×10^5 Nl/(kg_{cat} h) GHSV, feeding a gas mixture with 4% CH_4 (v/v), 2.24% O_2 (O_2/C = 0.56), and N_2 to balance. The conditioning procedure was considered complete when stable performances were achieved in the whole temperature range, typically within three runs. Only in one case, the conditioning procedure was skipped and the catalyst was first exposed directly to the standard C_3H_6 CPO conditions, which

consisted of 1% C_3H_6 (v/v), 1.68% O_2 (O_2/C = 0.56), N_2 to balance, and GHSV of 2×10^6 Nl/(kg_{cat} h). The effect of O_2 partial pressure was investigated, by performing experiments at higher O_2 concentration, from 1.68% up to 4.2% (O_2/C = 1.4) and keeping the C_3H_6 concentration constant at 1%. Steam reforming experiments were also carried out at 2×10^6 Nl/(kg_{cat} h) GHSV, with 0.5% C_3H_6 and 3% H_2O (v/v), corresponding to a steam to carbon ratio of 2. CH_4 CPO and C_3H_8 CPO experiments were also performed at 1% C concentration (corresponding to 3% CH_4, v/v and 1% C_3H_8, v/v), O_2/C ratio of 0.56, N_2 to balance and 2×10^6 Nl/(kg_{cat} h) GHSV.

2.3. Ex situ Raman experiments

The Raman experiments were carried out with a portable i-Raman BWTEK instrument (TE Cooled 2048 Pixel CCD detector). Laser excitation at 785 nm was used, with 5 cm^{-1} spectral resolution, and 175–3200 cm^{-1} shift range. The Raman instrument was connected to a video microscope sampling system (BAC151A) with integrated camera for tracking the laser beam position and focusing. The measurements were taken in backscattered mode.

In order to investigate the state of the catalyst surface during the reaction and monitor the production of carbon species, the Raman experiments were coupled with the CPO experiments. Indeed, in the annular reactor configuration, the very thin exposed catalyst layers and the transparent quartz glass allowed for a direct spectroscopic investigation of the catalyst surface. Fresh catalyst samples and conditioned catalysts were tested: the data on the fresh catalysts refer to CPO experiments and Raman measurements carried out during the very first run of the samples; the data on the conditioned catalysts refer to experiments that were performed after several runs under different operating conditions.

In the case of C_3H_6, Raman measurements were carried out during the first exposure of the fresh catalyst to a standard C_3H_6 CPO mixture, but also after a set of 40 runs (dedicated to the kinetic investigation). In the case of CH_4, Raman measurements were collected during the first exposure of the fresh catalyst to a CH_4 CPO conditioning mixture and also after the conditioning procedure had been completed.

The Raman measurements were taken at room temperature, according to the following procedure: (1) after reaching steady state in the annular reactor during the CPO test at a certain temperature, the gas mixture was switched to N_2 and the reactor was cooled down to room temperature, under inert N_2 flow; (2) the reactor, kept under N_2 flow, was extracted from the furnace and fixed to the adjustable table of the microscope; (3) the Raman signal was measured by focusing the beam directly on the catalyst layer through the quartz wall of the reactor, always kept under N_2 flow; (4) the gas mixture was switched back to the CPO composition, the reactor was inserted in the furnace and heated up to a new (higher) level of temperature. During each Raman inspection, five positions were scanned along the axis of the catalyst layer, by manually adjusting the movable table of the microscope. The first point was positioned at the very beginning of the layer, within the first millimeter, while the others were collected keeping a 5 mm gap between each other.

2.4. Temperature programmed oxidation tests

Temperature programmed oxidation (TPO) tests were also performed to quantify the amount of carbon accumulated on the catalyst during the CPO of C_3H_6 at three significant temperatures (300, 425 and 850 °C). The tests were carried out directly in the annular reactor, by heating the catalyst under air flow (GHSV = 10^4 Nl/(kg_{cat} h)) from room temperature up to 1000 °C at 2 °C/min, with a final hold of about 2 h. Prior to the TPO tests, the catalyst was exposed for 2 h to standard C_3H_6 CPO conditions and then cooled down to room temperature under inert N_2 flow. For each test, the results are reported as the ratio between the moles of CO_2 produced by combustion and the moles of Rh present in the catalyst (2.4 μmol).

3. Results and discussion

3.1. Kinetic dependences: investigation in annular reactor

In order to better appreciate the features observed in the CPO of C_3H_6, it is worthy to first recall the main characteristics of the CPO process with CH_4 and C_3H_8. CH_4 is the reference hydrocarbon in CPO and, by far, the most broadly studied, while C_3H_8 is herein taken into consideration as it is the saturated homologue of C_3H_6. Additionally, in our experience, the reactivity patterns of CH_4 and C_3H_8 are widely representative of the CPO of light alkanes. A comparison is proposed in Fig. 1 between the results of CPO tests performed with CH_4 (panel a) and C_3H_8 (panel b). The comparison is realized at equal contact time and C concentration in the reacting gas mixture. The conversion of O_2 and fuel, and the molar fractions of H_2 and H_2O are plotted as a function of the temperature. The total oxidation of CH_4 activates around 300 °C and goes to completion at ~460 °C, as indicated by the O_2 conversion curve. In the presence of O_2, H_2O and CO_2 are the only products observed. Upon increasing the temperature, a smooth transition between the total oxidation regime and the oxidation plus steam reforming regime is observed: once O_2 reaches the complete consumption, steam reforming effectively consumes the fuel and the H_2O, with production of syngas and with steady increase of the fuel conversion with temperature and contact time. An almost identical evolution is observed in the case of C_3H_8: the total oxidation region starts at 300 °C and completes the conversion of O_2 at ~400 °C, above which we observe the activation of steam reforming, responsible for the production of syngas and eventually for the complete conversion of the fuel.

The analogy between CH_4 and C_3H_8 CPO is further strengthened by the kinetic dependencies observed. As reported in previous works [27,28], CPO experiments performed at nonstoichiometric O_2/C ratios reveal that the rate of total oxidation is independent from the concentration of O_2 and first order dependent on the fuel concentration. Zeroth-order equations are therefore proposed with respect to O_2 for both CH_4 and C_3H_8. The independence from O_2 suggests that the activation of CH_4 and C_3H_8 occurs in the presence of similar surface coverages, namely on a surface saturated by chemisorbed oxygen atoms O^*. With reference to the kinetic studies of Iglesia and co-workers for methane and ethane on noble metal catalysts [29,30], the activation of CH_4 and C_3H_8 would then occur in the so-called Regime I, that is, by dissociation of the C–H bond on chemisorbed oxygen pairs. Important similarities between CH_4 and C_3H_8 emerge also for the steam reforming: in both cases, experiments at low fuel conversion (<20%) show that the intrinsic rate of the reaction is first-order with respect to the concentration of the fuel and comparable with the rate of total oxidation. As a matter of fact, the steam reforming rate is found independent of the co-reactant concentration (i.e. H_2O), thus indicating that the activation of the fuel is again the determining step. Additionally, for both CH_4 and C_3H_8, at higher conversion, it is experimentally found that O_2 delays the activation of steam reforming and that the global order of the reaction appears to be lower than 1: coherently, in order to describe these effects, inhibition terms due to O_2 and CO adsorption are assumed in lumped rate equations [27,28].

The results of a typical C_3H_6 CPO test carried out under isothermal conditions in the annular reactor are presented in Fig. 2. The conversion of the reactants and the molar fraction of the products are plotted as a function of temperature. Taking into consideration the characteristics of CH_4 and C_3H_8 CPO, significant differences

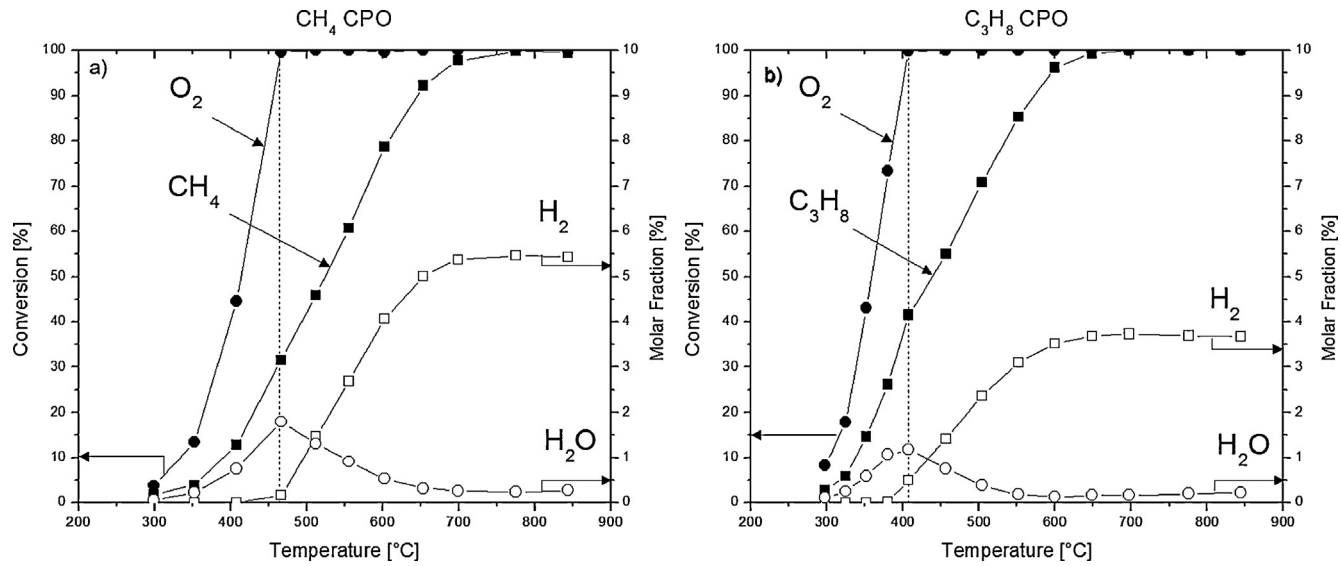

Fig. 1. Comparison among CPO experiments with different fuels. $O_2/C = 0.56$ and GHSV = 2×10^6 Nl/(kg_{cat} h). Fuel and O_2 conversion are reported. Panels: (a) CH_4 = 3% (v/v); (b) C_3H_8 = 1% (v/v). Full symbols are conversion of the fuel (■) and O_2 (●). Open symbols are molar fraction of H_2 (□) and H_2O (○).

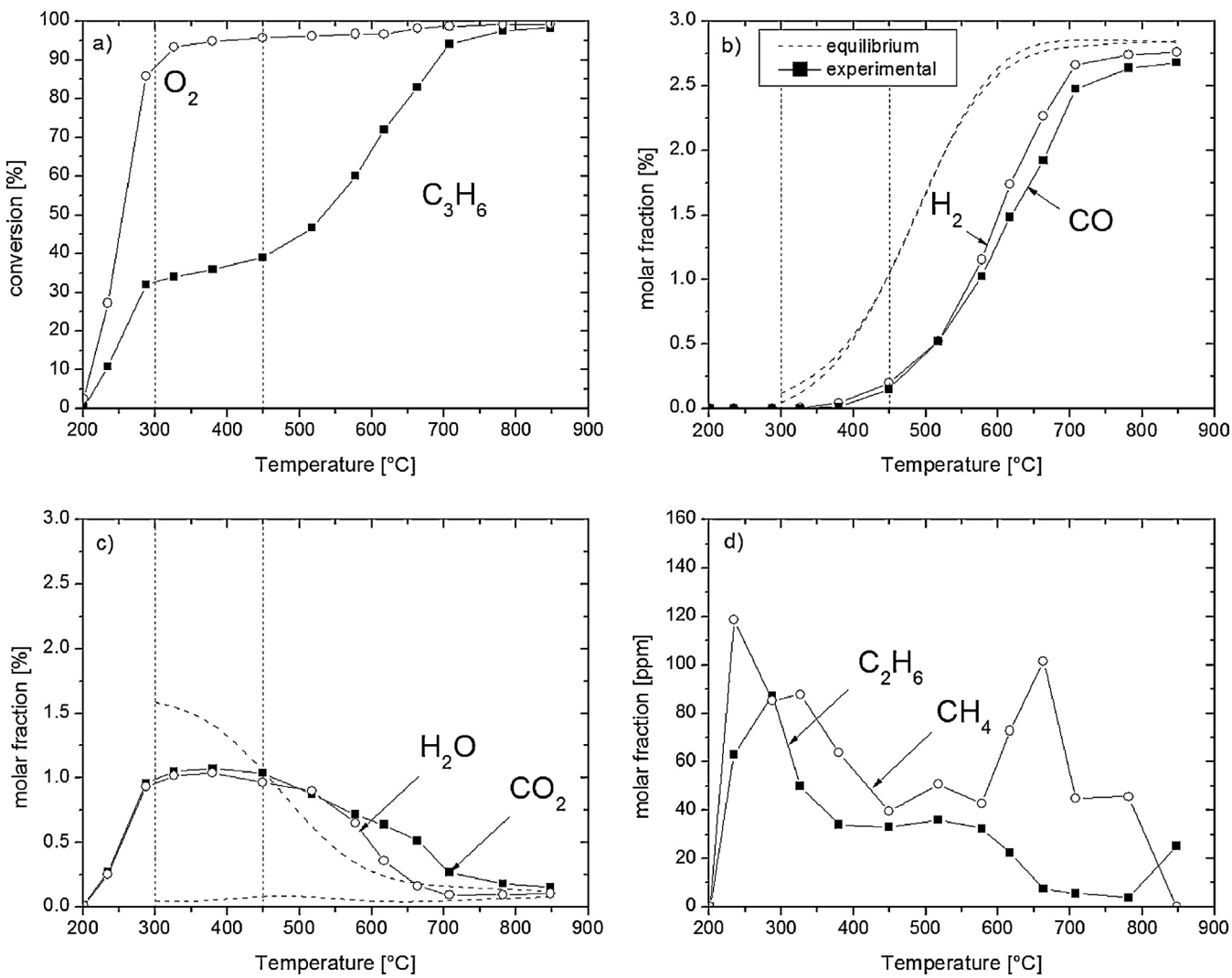

Fig. 2. C_3H_6 CPO experiment. C_3H_6 = 1% (v/v), O_2 = 1.68%, N_2 to balance, $O_2/C = 0.56$, GHSV = 2×10^6 Nl/(kg_{cat} h), P = 1 atm. Panels: (a) conversion of O_2 and C_3H_6; (b) molar fraction of H_2 and CO; (c) molar fraction of H_2O and CO_2; (d) molar fraction of C_2H_6 and CH_4. Symbols are data. Dashed lines are equilibrium.

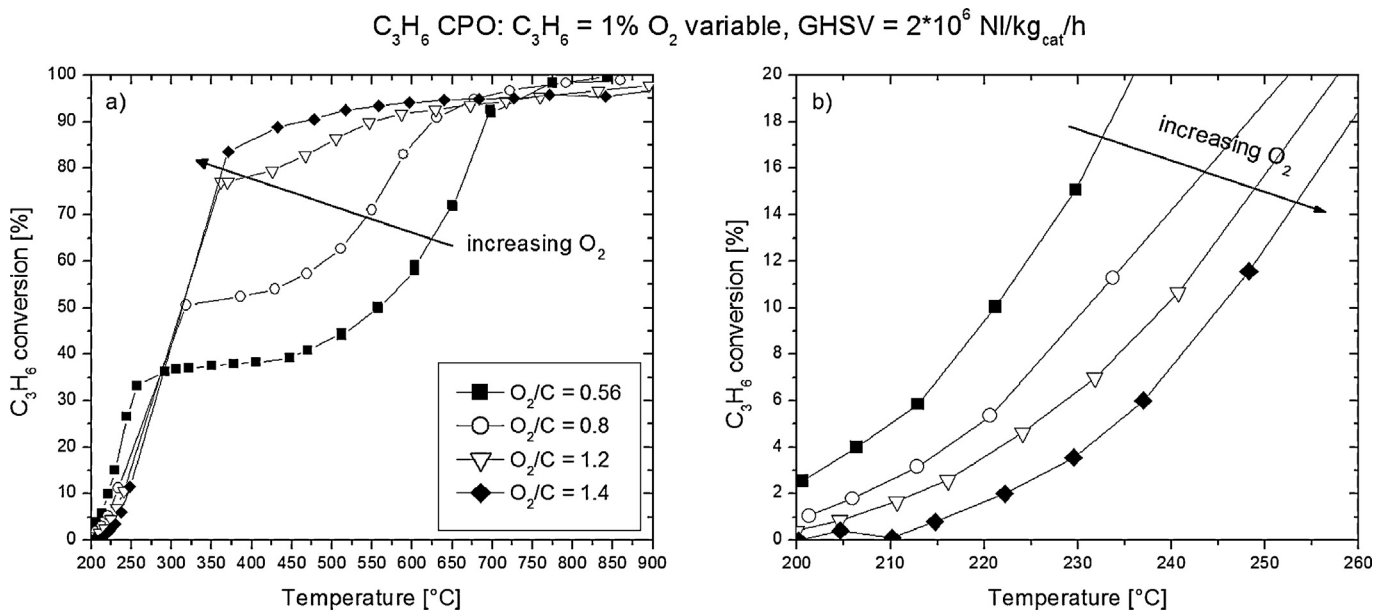

Fig. 3. Effect of O_2 concentration in C_3H_6 CPO. C_3H_6 = 1% (v/v), $O_2/C = 0.56 \rightarrow 1.4$, N_2 to balance, GHSV = 2×10^6 Nl/(kg_{cat} h). Panel (b) is a zoom.

emerge. At remarkably low temperature, between 200 and 300 °C, C_3H_6 reacts with O_2 producing exclusively CO_2 and H_2O. No synthesis gas is formed, in line with the activation of the total oxidation reaction (Eq. (1)). Compared to CH_4 and C_3H_8, the total oxidation of C_3H_6 is therefore extremely faster: it activates almost 100 °C lower and reaches 95% of O_2 conversion at 350 °C, when CH_4 and C_3H_8 total oxidation has just started.

$$C_3H_6 + 9/2O_2 \rightarrow 3CO_2 + 3H_2O \quad (1)$$

Between 300 and 400 °C, once the conversion of O_2 is nearly complete (>90%), the conversion of C_3H_6 slowly increases from 35% to 40%, with further production of CO_2 and H_2O and very limited formation of syngas, around 400 °C. At temperatures higher than 400 °C, the conversion of C_3H_6 steadily increases up to complete consumption, at the expenses of H_2O, with steady production of H_2 and CO, according to the steam reforming reaction (Eq. (2)). Conversion of CO_2 is also observed and attributed to the onset of the reverse water gas shift reaction (Eq. (3)). Differently from the early activation of total oxidation, the steam reforming of C_3H_6 activates in a temperature range (400–450 °C) comparable with that of CH_4 and C_3H_8 (dashed lines in Fig. 1), but initially progresses with a slow rate, as suggested by the slope of C_3H_6 conversion curve between 450 and 600 °C.

$$C_3H_6 + 3H_2O \rightarrow 3CO + 6H_2 \quad (2)$$

$$H_2 + CO_2 \rightarrow CO + H_2O \quad (3)$$

In the whole temperature range, production of trace quantities of CH_4 and C_2H_6 is also observed (Fig. 2d), likely due to the occurrence of surface cracking reactions involving C_3H_6. The extent of these reactions is extremely limited, nonetheless a catalytic route is possibly active at low temperatures, which could explain the production of CH_4 and C_2H_6 below 450 °C, while a homogenous route could prevail at higher temperatures.

Further details on the individual reaction kinetics observed in C_3H_6 CPO will be given in the dedicated companion paper. Herein, it is important to note that a remarkable distinction emerges between the ultra-fast total oxidation activity and the steam reforming activity, which results in a discontinuity and in the appearance of a plateau in the conversion of C_3H_6. Compared to CH_4 and C_3H_8, whose transition between the total oxidation and the steam reforming regimes is smooth, such a discontinuity is a unique feature. In the literature, other authors [31] reported the occurrence of a similar plateau when performing the partial oxidation of propane over Pt and Pt–Ce catalysts, under conditions close to the present ones. The behavior was associated to the difference between the rate of total oxidation and that of steam reforming, which was reported to be delayed on Pt surfaces by the inhibiting effect of water. However, in the present case, the reactivity of C_3H_6, which is an olefin and has an unsaturated double bond, suggests that different kinetic dependencies may cause the observed behavior, with particular reference to the adsorption characteristics.

In light of this, it is worthy to analyze the main kinetic dependences of the total oxidation and the steam reforming rate. In the first case, a C_3H_6 CPO experiment is presented in Fig. 3, performed by increasing the O_2 to C ratio while keeping the concentration of C_3H_6 constant. The increase of O_2 concentration shifts the plateau to higher conversion levels, finally leading to its disappearance at $O_2/C = 1.4$. In contrast, in the low temperature and low conversion region ($T < 260$ °C), an inhibition effect on C_3H_6 conversion is observed: indeed, at increasing O_2 concentration, the conversion of C_3H_6 decreases. The inhibiting effect of O_2 on C_3H_6 conversion suggests competing adsorption between the two reactants, and, in turn, that the surface is possibly covered by both chemisorbed oxygen and CH_x hydrocarbon intermediates deriving from C_3H_6 activation. Again, with reference to Ref. [29], we propose that the activation of C_3H_6 in the presence of O_2 in CPO occurs in a kinetic regime similar to what the authors identify as Regime II, i.e. the activation of the hydrocarbon on vacancies coupled with chemisorbed oxygen (O*–* pairs).

Along with the high affinity of C_3H_6 for the Rh surface, steam reforming tests (Fig. 4) show that the reaction activates at temperatures around 500 °C, higher than those observed in the high temperature branch of the CPO experiment, and much higher than those found on the same catalyst under comparable conditions in case of CH_4 (~300 °C) and C_3H_8 (~350 °C) [27,28]. Notably, neither hydrogen nor methane and ethylene are observed before the reaction starts, possibly indicating that cracking is not occurring under steam reforming conditions. Such a delayed activation suggests the occurrence of a self-inhibiting effect of C_3H_6, which sticks on the catalyst surface, saturates the active sites and prohibits the adsorption of H_2O up to the reaching of sufficiently high temperatures.

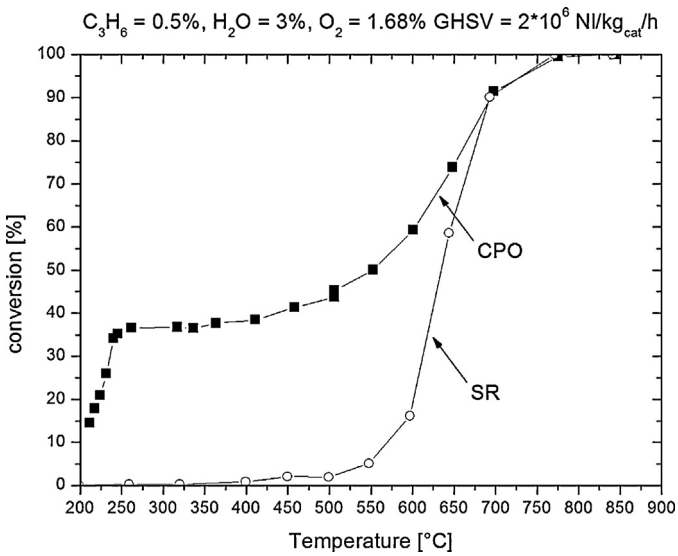

Fig. 4. Comparison between the conversion of C_3H_6 in CPO and Steam Reforming. C_3H_6 = 0.5% (v/v), O_2/C = 0.65 (CPO), H_2O/C = 2 (SR), GHSV = 2×10^6 Nl/(kg_{cat} h).

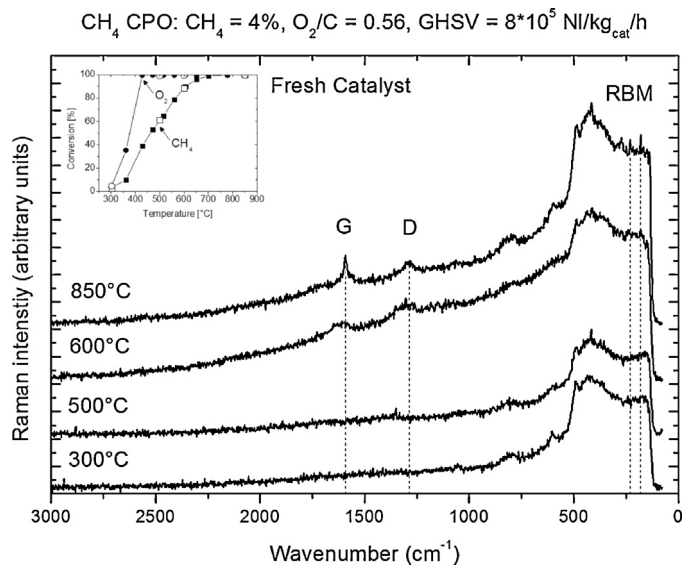

Fig. 5. Raman measurements during CH_4 CPO over a fresh catalyst. CH_4 = 4% (v/v), O_2 = 2.24%, N_2 to balance, O_2/C = 0.56, GHSV = 8×10^5 Nl/(kg_{cat} h), P = 1 atm. Insert: conversion of CH_4 (■, □) and O_2 (●, ○) as a function of temperature.

Overall, the kinetic tests performed in the annular reactor point out that the reactivity of C_3H_6 is strongly characterized by its high adsorption capability on the Rh surface, which results in a quicker activation of the total oxidation reaction, but blocks the surface in the case of steam reforming. As a consequence of the sticking capability of C_3H_6, it is interesting to understand what is the state of the surface during the CPO and whether carbon residues are accumulated, which can potentially lead to the coking of the catalyst. Thanks to its sensitivity to carbon structures, Raman analysis of the surface was individuated as a potentially suitable tool. Carbon accumulation appears to play an important role, given that the catalyst slowly deactivates over the course of repeated standard C_3H_6 CPO tests.

3.2. *Ex situ Raman investigation of the catalyst surface*

The state of the catalyst surface was investigated during two reference situations at equal O_2/C ratio of 0.56, namely the standard C_3H_6 CPO experiment (1%, v/v C_3H_6 and 2×10^6 Nl/(kg_{cat} h) GHSV) and a CH_4 CPO experiment under the typical conditions adopted in kinetic tests (4%, v/v CH_4 and 8×10^5 Nl/(kg_{cat} h) GHSV). As well, the Raman experiments were performed over two different surfaces, the fresh surface, characteristic of the catalyst at its first exposure to the reacting mixture, and the conditioned surface, representative of the surface after reasonable time on stream. The experimental procedure adopted in the measurements is detailed in Section 2.3. In all cases, the same CPO run was repeated after the Raman test, in order to verify the occurrence of possible changes of the catalytic activity. The observed variations were within the experimental uncertainty, suggesting that the procedure had no significant side effects. In the figures that report the Raman spectra (Figs. 5–8), inserts are present that plot the fuel conversion as a function of temperature during (open symbols □) and after (full symbols ■) the Raman measurements. Only in the case of the fresh sample exposed to C_3H_6 CPO conditions (Fig. 7, insert), the comparison is provided between the conversion obtained during the Raman test and that obtained over the fully conditioned catalyst of Fig. 2. It can be seen that, aside of moderate variations of the activity, all the characteristic features are retained. It is also worthy to note that the Raman spectra reported in the figures were those collected in the middle of the catalyst layer, which represent a reasonable average over the intensity fluctuations. Along the layer, at each temperature, the same peaks were always identified, but with different intensities. These differences are related to the reaction chemistry and are discussed in Section 3.3.

The results of the Raman investigation performed during CH_4 CPO over a fresh surface are reported in Fig. 5. Up to 500 °C, no signal associated to carbon is detected. At 600 °C, when O_2 is totally converted and CH_4 is consumed by steam reforming, weak signals at 1595 cm^{-1} and 1350 cm^{-1} appear, respectively attributed to the formation of graphitic structures (peak G) and amorphous carbon deposits (peak D). Even though the unambiguous attribution of peak D is still debated, for the purpose of this work it can be confidently associated to the presence of amorphous carbon deposits and, more generally, of condensed poly-aromatic moieties embedded in amorphous regions [32] or edge-regions of ordered graphitic structures [33]. At 850 °C, when the reaction reaches the complete conversion, the G and D peaks are accompanied by lines typically

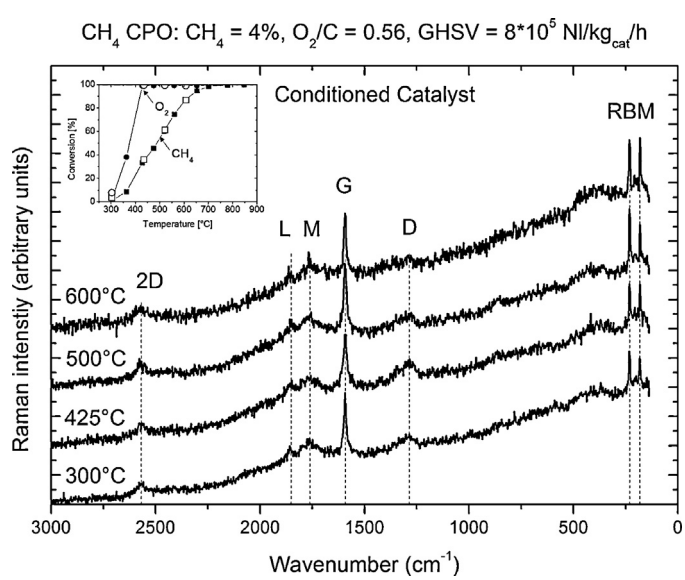

Fig. 6. Raman measurements during CH_4 CPO over a conditioned catalyst. CH_4 = 4% (v/v), O_2 = 2.24%, N_2 to balance, O_2/C = 0.56, GHSV = 8×10^5 Nl/(kg_{cat} h), P = 1 atm. Insert: conversion of CH_4 (■, □) and O_2 (●, ○) as a function of temperature.

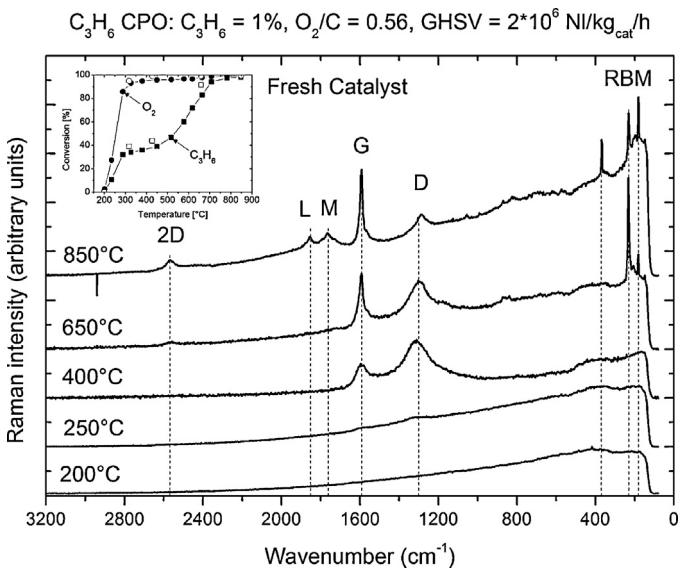

Fig. 7. Raman measurements during C_3H_6 CPO over a fresh catalyst. C_3H_6 = 1% (v/v), O_2 = 1.68%, N_2 to balance, O_2/C = 0.56, GHSV = 2×10^6 Nl/(kg_{cat} h), P = 1 atm. Insert: conversion of C_3H_6 (■, □) and O_2 (●, ○) as a function of temperature.

associated to the formation of carbon nanotubes, i.e. the radial breathing modes of the nanotubes (RBM, 400–180 cm^{-1} region) and the sharp component of the G peak. The formation of carbon nanotubes (previously reported on Rh foils [34]) suggests that more organized structures are present on the surface at high temperatures. Nonetheless, as generally experienced with noble metals, these results confirm that CH_4 has a low sticking tendency and hence also a low tendency to form and accumulate carbonaceous species on the catalyst surface, which maintains relatively clean during the CPO reaction. As a matter of fact, the CPO of CH_4 on Rh-based catalysts is known to proceed with no coking issues also at higher CH_4 concentration and more challenging conditions than the present ones, for instance with CH_4/air streams within autothermal reformers [35–37].

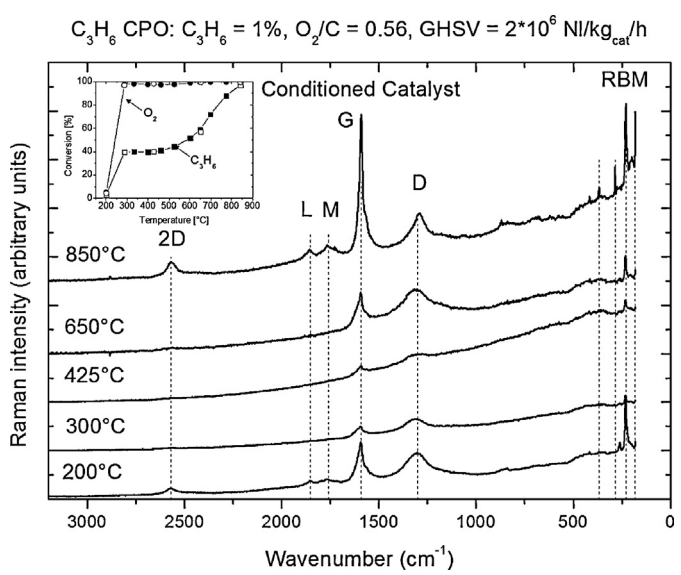

Fig. 8. Raman measurements during C_3H_6 CPO over a conditioned catalyst. C_3H_6 = 1% (v/v), O_2 = 1.68%, N_2 to balance, O_2/C = 0.56, GHSV = 2×10^6 Nl/(kg_{cat} h), P = 1 atm. Insert: conversion of C_3H_6 (■, □) and O_2 (●, ○) as a function of temperature.

Different features appear in the Raman spectra collected during the CH_4 CPO test over the conditioned catalyst (Fig. 6). At 300 °C, when the conversion of CH_4 and O_2 has not yet started, a sharp G peak, a weak D peak and the RBM signals of the nanotubes [38] are already present. The latter low frequency Raman features characteristic of nanotubes are consistent with the diameters of the tubes which can be probed with the 785 nm excitation in a Kataura plot [38] and are well distinguished from the low frequency Raman features of other sp^2 carbon species like onions [39] or C_{60} buckyball [40]. Some other signals are also distinguished at 2567 cm^{-1} (2D peak [41]), 1850 cm^{-1} (L peak [42,43]) and 1780 cm^{-1} (M features [44]), which can be respectively attributed to the first overtone of the D peak (associated to the formation of extended polycyclic aromatic structures), to linear carbon chains (polyynes) and overlapped contributions from nanotubes and graphite. The appearance of these signals at low temperature is due to the accumulation of the carbon species formed at high temperature during the previous conditioning runs. This accumulation is a direct consequence of the conditioning process, which involves loss of defect sites on the surface and ends up with the establishment of a steady-state limited amount of C-species that does not hinder the activity and the life of the catalyst [26,45]. The experimental procedure followed (Section 2) allowed to preserve this C-species also at low temperature: indeed, between each run and the next one, the catalyst is cooled to ambient temperature under inert N_2 atmosphere, so as to keep the state of the surface intact. Upon increasing the temperature to 600 °C, the Raman spectra show that the G and the RBM signals become sharper, while the other peaks weaken or disappear. The final state of the surface is again relatively clean, in line with the results obtained over the fresh catalyst and with the widely recognized stability of CH_4 CPO on Rh. Along with this, it is worthy to note that the signal to noise ratio of the spectra, which in both cases have irregular profiles, can be assumed as an additional piece of evidence of the limited amount of carbon present on the catalyst. Overall, the Raman measurements over the fresh and the conditioned catalysts are consistent with the kinetic dependences discussed in Section 3.1: the surface is almost fully available, so that, once O_2 is consumed, the steam reforming of CH_4 proceeds with high rate and with no temperature gap between the oxidation and the reforming branch (Fig. 1a).

A more elaborate picture emerges from the Raman experiments performed during C_3H_6 CPO. The results obtained over the fresh catalyst are reported in Fig. 7. No carbon signals are detected up to 200 °C, when O_2 conversion is low (insert). Already at 300 °C, at the beginning of the flat region, weak G and D peaks appear, which grow considerably at 425 °C. Notably, at 300 °C the conversion of O_2 still amounts to 85% only. At 650 °C, when the steam reforming is active, the RBM lines and the sharp G component of the nanotubes are observed. At 850 °C, the G and RBM signals become sharper and the D peak weakens. The 2D, L and M signals are also evident. Clearly, carbon intermediates of complex nature are formed on the catalyst surface during the CPO of C_3H_6, in line with the pronounced affinity of C_3H_6 with the Rh surface and with the carbon accumulation tendency of the catalyst.

When the Raman measurements are repeated over a fully conditioned catalyst (Fig. 8), some differences are found. In line with the accumulation effect discussed in the case of CH_4 CPO and related to the experimental procedure, the spectra collected at 200 °C show a pattern essentially analogous to those observed at 850 °C on the fresh surface. Differences are noted in the contributions of peak D and of the RBMs, which are reasonably due to the fact that the catalyst underwent a series of runs at various operating conditions, also with non-stoichiometric C_3H_6/O_2 mixtures. Most importantly, however, when the temperature is increased to 300 °C, only weak D and G peaks are present, while all the other signals (2D, L, M and RBM) have disappeared. This result is likely due to the cleaning

Table 1
Results of TPO tests performed after standard C_3H_6 CPO experiments at three different temperatures. The C/Rh ratio is estimated as the moles of CO_2 produced by combustion divided by the total amount of Rh present in the catalyst (2.4 μmol).

CPO T [°C]	CO_2 [μmol]	C/Rh ratio
300	31.2	13
425	135.0	56
850	36.6	15

effect of O_2, which burns off most of the "inherited" carbon deposits and keeps a favorable C balance, avoiding a severe build-up: as a consequence, the spectra are similar to those obtained over the fresh surface at equal temperature (Fig. 7), even though the initial condition is different. The evolution of the Raman spectra from 425 °C to 850 °C confirms that of the fresh catalyst: a significant growth of D and G peaks is observed, followed by the strengthening of the RBM signals and to the appearance of the 2D, L and M signals at 850 °C.

Taken together, these results seem to agree with the kinetic dependences outlined by the experiments in the annular reactor, and also with the results of the TPO tests performed after the C_3H_6 CPO experiments (Table 1). The strong adsorption of C_3H_6 leads to the build-up of carbon species: at low temperatures and low O_2 partial pressure, carbon species are observed even in the presence of unconverted O_2 (Fig. 2a and insert in Fig. 7), as suggested by the spectra at 300 °C (Figs. 7 and 8) and by the production of ppm amounts of CH_4 and C_2H_6 between 200 and 300 °C (Fig. 2d). Coherently, a low amount of carbon (C/Rh ratio of 13 mol/mol) is found after the CPO experiment at 300 °C. At intermediate temperatures, the adsorption of C_3H_6 followed by formation of relatively stable C species, mainly amorphous, hinders the surface sites and delays the formation of synthesis gas by steam reforming. High temperatures are then required to unblock the surface and allow for the full activation of the steam reforming reaction. In line with this picture, the highest amount of carbon (56 mol/mol) is found after the CPO at 425 °C, indicating that the build-up of carbon mostly occurs in the absence of O_2 and when C_3H_6 steam reforming is barely active. Upon increasing the temperature to 850 °C, the C/Rh ratio drops to 15 mol/mol: a carbon removal mechanism is therefore active, which is possibly associated with the gasification by H_2O and the formation of synthesis gas.

3.3. Hypotheses on carbon removal mechanism

Given the key role of the adsorbed intermediates in the reactivity of C_3H_6, it is interesting to investigate the mechanism that removes the carbon species and unblocks the Rh surface. First, it is important to note that, upon increasing the temperature, an evolution is observed in the carbon structures, which start from amorphous deposits and go to nanotubes, therefore following the direction of increasing order. Such an evolution is better appreciated by quantitative estimation of the ratio between the intensity of the D and G peaks of each Raman spectra collected during the test. This ratio can indeed be taken as an indicator of the increasing or decreasing disorder of the carbon structures, and, in other words, of the maturity of the C-complexes present on the surface. The ratio between peak D and G calculated during the C_3H_6 CPO test over the fresh catalyst is reported as a function of temperature in Fig. 9: a constant decrease is observed at increasing temperature. This result suggests that a chemical mechanism is active on the surface, but does not entirely clarify its nature. In fact, it is commonly understood that more disordered carbon structures are also more reactive than ordered ones, thanks to the higher number of edges and active sites: consequently, any C-consuming reaction (combustion, inverse CO disproportionation or gasification) would deplete the amorphous carbon first and cause a decrease of the D/G ratio. As well, the occurrence of a route that reorganizes the amorphous structures into ordered complexes (nanotubes and graphite), unblocking the occupied sites, cannot in principle be excluded. This route would be driven by temperature and could possibly work in parallel to the C-consuming route.

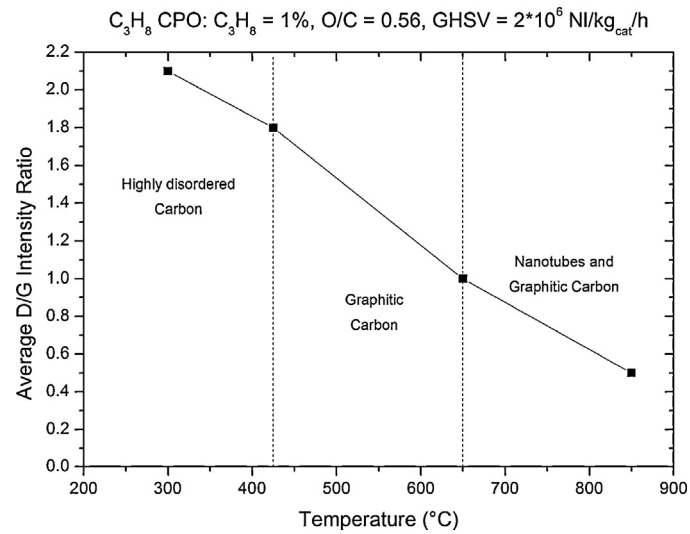

Fig. 9. Average D/G intensity ratio as a function of temperature.

A more detailed picture is given by the analysis of the axial profiles of the D/G ratio collected by scanning the catalyst layer. For each different temperature, the profiles are reported in Fig. 10 as a function of the axial position. At 300 and 425 °C the D/G ratio is fairly constant along the layer, while at 650 and 850 °C a common evolution is found, wherein the ratio first keeps almost constant (points 1 and 2) and then grows steadily up to the outlet of the layer (points 3–5). These results can be reasonably interpreted on the basis of the axial profiles of gas phase composition encountered during the isothermal CPO tests. Up to 425 °C, C-combustion determines the D/G ratio: indeed, almost no synthesis gas is produced (Fig. 2b), CO_2 and H_2O are the only relevant products (Fig. 2c) and O_2 is not completely consumed (at 300 °C) or it is totally consumed right by the end of the catalyst (at 425 °C, 98% O_2 conversion). At 650 and 850 °C, the evolution of the D/G ratio is associated with the

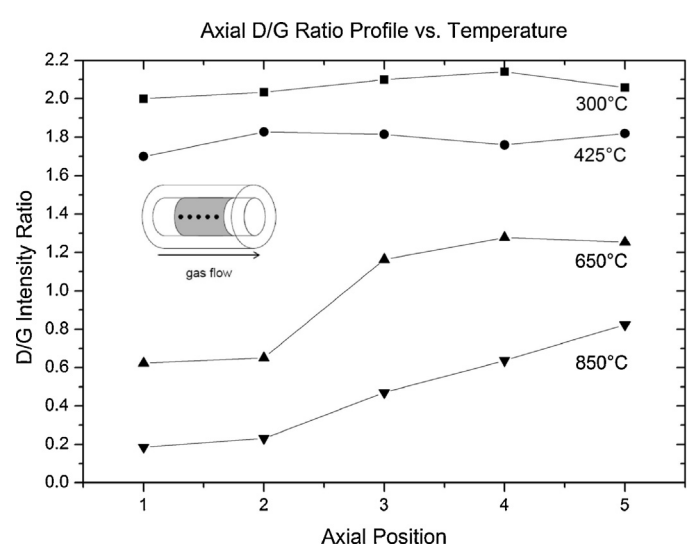

Fig. 10. D/G intensity ratio as a function of axial position. Raman measurements are taken after C_3H_6 CPO tests at: 300 °C (■); 425 °C (●); 650 °C (▲); 850 °C (▼).

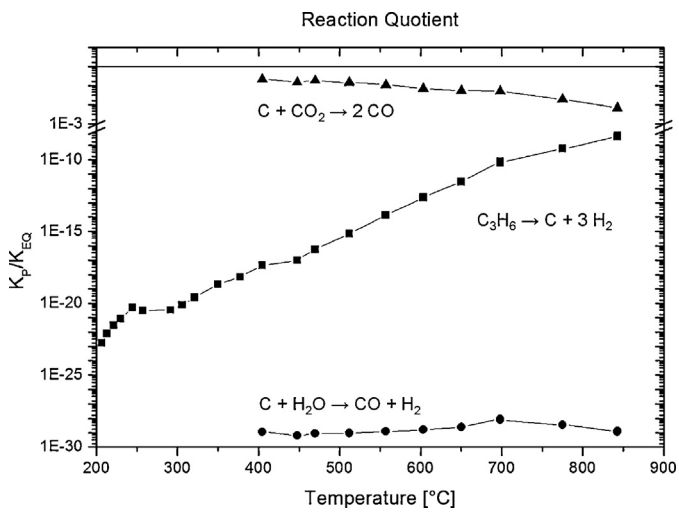

Fig. 11. Reaction quotients: C_3H_6 cracking (■); Carbon gasification (▲); Inverse CO disproportionation (●).

onset of an oxidation zone, followed by a reforming zone wherein syngas is produced. In the first part of the catalyst, O_2 is still present and is being consumed, and C-combustion prevails. In this respect, it is worthy to note that the distance between the scanned points is not exact and regular due to manual positioning of the measuring spot, so that the distances in the graph are not representative of the expected O_2 consumption lengths. In the second part of the layer, O_2 is completely consumed and H_2O and CO are responsible for the removal of C species, anyway less efficiently than O_2, as suggested by the increase of the D/G ratio. In this case, gasification (Eq. (4)) and inverse CO disproportionation (Eq. (5)) could be the active routes for C removal. Consistently, the estimation of the reaction quotients K_P/K_{EQ} (Fig. 11) shows that, under the investigated conditions, carbon gasification and inverse CO disproportionation are both thermodynamically favored, with the latter reaction being much closer to the equilibrium than the first one. As expected, the reaction quotients also evidence that the C_3H_6 cracking route (Eq. (6)) could be responsible for C production at all temperatures.

$$C + H_2O \rightarrow CO + H_2 \quad (4)$$

$$C + CO_2 \rightarrow 2CO \quad (5)$$

$$C_3H_6 \rightarrow 3C + 2H_2 \quad (6)$$

Overall, the thermodynamic analysis and the analysis of the D/G ratios tell that, in the absence of O_2, CO and mostly H_2O may have a role in the removal of carbon species, respectively via carbon disproportionation and gasification.

4. Conclusions

Olefins are byproducts of the catalytic partial oxidation of LPG and higher alkanes, which can significantly impact the reaction, eventually leading to the deactivation of the catalyst by formation of carbon deposits. In the present work, the behavior of propylene in the CPO reaction conducted over 2 wt% Rh/α-Al_2O_3 catalysts is analyzed with attention to its carbon-formation tendency, by coupling the kinetic analysis in an annular microreactor with the ex situ Raman investigation of the catalyst surface. A comparison is provided with the behavior of CH_4, assumed as the coke-free reference fuel for CPO. The high affinity of C_3H_6 for the metal surface clearly emerges from the kinetic tests: at low temperatures (<350 °C), a competition between the adsorption of C_3H_6 and O_2 is observed, which results in the fast activation of the total oxidation reaction; at higher temperatures, adsorption of C_3H_6 almost saturates the metal surface, blocking the adsorption of the co-reactant and strongly inhibiting the formation of synthesis gas by steam reforming. Ex situ Raman experiments performed during the CPO reaction reveal that different carbonaceous species are present on the catalyst surface as a consequence of the adsorption of C_3H_6: an evolution is observed upon increasing the temperature, which starts from amorphous carbon deposits, passes through the formation of graphitic structures and completes with the appearance of nanotubes. Comparatively, the analogous experiments performed with CH_4 reveal a much cleaner surface, in line with the lower sticking capability and the lower coking tendency. The evolution observed in C_3H_6 CPO follows the direction of increasingly ordered C-structures and indicates that a mechanism, driven by gas-phase reactants and by temperature, is active, which unblocks the Rh surface from carbon-based adsorbates and allows for the steam reforming to occur. The analysis of the Raman spectra collected along the axis of the catalyst layer provide a picture of the chemical routes involved: below 350 °C, in the presence of O_2, highly disordered amorphous carbon exclusively forms due to oxidation reactions. When syngas is produced (T > 450 °C) and the consumption of O_2 is confined to a portion of the catalyst layer, carbon gasification and inverse CO disproportionation are responsible for C removal.

References

[1] D. Livio, A. Donazzi, A. Beretta, G. Groppi, P. Forzatti, Ind. Eng. Chem. Res. 51 (2012) 7573–7583.
[2] D. Livio, A. Donazzi, A. Beretta, G. Groppi, P. Forzatti, Top. Catal. 54 (2011) 866–872.
[3] I. Aartun, T. Gjervan, H. Venvik, O. Gorke, P. Pfeifer, M. Fathi, A. Holmen, K. Schubert, Chem. Eng. J. 101 (2004) 93–99.
[4] I. Aartun, B. Silberova, H. Venvik, P. Pfeifer, O. Gorke, K. Schubert, A. Holmen, Catal. Today 105 (2005) 469–478.
[5] I. Aartun, H.J. Venvik, A. Holmen, P. Pfeifer, O. Gorke, K. Schubert, Catal. Today 110 (2005) 98–107.
[6] N.J. Degenstein, R. Subramanian, L.D. Schmidt, Appl. Catal. A: Gen. 305 (2006) 146–159.
[7] O. Deutschmann, M. Hartmann, L. Maier, Appl. Catal. A: Gen. 391 (2011) 144–152.
[8] O. Deutschmann, M. Hartmann, L. Maier, H.D. Minh, Combust. Flame 157 (2010) 1771–1782.
[9] O. Deutschmann, L. Maier, M. Hartmann, S. Tischer, Combust. Flame 158 (2011) 796–808.
[10] B.J. Dreyer, P.J. Dauenhauer, R. Horn, L.D. Schmidt, Ind. Eng. Chem. Res. 49 (2010) 1611–1624.
[11] B.J. Dreyer, I.C. Lee, J.J. Krummenacher, L.D. Schmidt, Appl. Catal. A: Gen. 307 (2006) 184–194.
[12] M. Hartmann, T. Kaltschmitt, O. Deutschmann, Catal. Today 147 (2009) S204–S209.
[13] M. Huff, P.M. Torniainen, L.D. Schmidt, Abstr. Papers Am. Chem. Soc. 206 (1993) 127–130.
[14] J.J. Krummenacher, K.N. West, L.D. Schmidt, J. Catal. 215 (2003) 332–343.
[15] G.J. Panuccio, B.J. Dreyer, L.D. Schmidt, AIChE J. 53 (2007) 187–195.
[16] L.D. Schmidt, E.J. Klein, C.A. Leclerc, J.J. Krummenacher, K.N. West, Chem. Eng. Sci. 58 (2003) 1037–1041.
[17] L. Basini, Catal. Today 117 (2006) 384–393.
[18] M.A. Banares, Catal. Today 51 (1999) 319–348.
[19] V.D. Sokolovskii, Catal. Today 24 (1995) 377–381.
[20] A. Beretta, T. Bruno, G. Groppi, I. Tavazzi, P. Forzatti, Appl. Catal. B: Environ. 70 (2007) 515–524.
[21] O. Korup, R. Schlogl, R. Horn, Catal. Today 181 (2012) 177–183.
[22] A. Donazzi, D. Livio, M. Maestri, A. Beretta, G. Groppi, E. Tronconi, P. Forzatti, Angew. Chem. Int. Ed. 50 (2011) 3943–3946.
[23] B.E. Bent, C.M. Mate, J.E. Crowell, B.E. Koel, G.A. Somorjai, J. Phys. Chem. 91 (1987) 1493–1502.
[24] M.J. Calhorda, P.E.M. Lopes, C.M. Friend, J. Mol. Catal. A Chem. 97 (1995) 157–171.
[25] X.P. Xu, C.M. Friend, J. Am. Chem. Soc. 112 (1990) 4571–4573.
[26] A. Beretta, A. Donazzi, G. Groppi, P. Forzatti, V. Dal Santo, L. Sordelli, V. De Grandi, R. Psaro, Appl. Catal. B Environ. 83 (2008) 96–109.
[27] A. Donazzi, A. Beretta, G. Groppi, P. Forzatti, J. Catal. 255 (2008) 241–258.
[28] D. Pagani, D. Livio, A. Donazzi, A. Beretta, G. Groppi, M. Maestri, E. Tronconi, Catal. Today 197 (2012) 265–280.
[29] M. Garcia-Dieguez, Y.H. Chin, E. Iglesia, J. Catal. 285 (2012) 260–272.
[30] J.M. Wei, E. Iglesia, J. Catal. 225 (2004) 116–127.
[31] J. Barbier, D. Duprez, Appl. Catal. A: Gen. 85 (1992) 89–100.

[32] C. Castiglioni, M. Tommasini, G. Zerbi, Philos. Trans. R. Soc. Lond. Ser. A Math. Phys. Eng. Sci. 362 (2004) 2425–2459.
[33] M. Tommasini, C. Castiglioni, G. Zerbi, A. Barbon, M. Brustolon, Chem. Phys. Lett. 516 (2011) 220–224.
[34] J.K. Chinthaginjala, S. Unnikrishnan, M.A. Smithers, G.A.M. Kip, L. Lefferts, Carbon 50 (2012) 1434–1437.
[35] A. Donazzi, B.C. Michael, L.D. Schmidt, J. Catal. 260 (2008) 270–275.
[36] R. Horn, K.A. Williams, N.J. Degenstein, A. Bitsch-Larsen, D.D. Nogare, S.A. Tupy, L.D. Schmidt, J. Catal. 249 (2007) 380–393.
[37] R. Schwiedernoch, S. Tischer, C. Correa, O. Deutschmann, Chem. Eng. Sci. 58 (2003) 633–642.
[38] M.S. Dresselhaus, G. Dresselhaus, R. Saito, A. Jorio, Phys. Rep. Rev. Sec. Phys. Lett. 409 (2005) 47–99.
[39] D. Roy, M. Chhowalla, H. Wang, N. Sano, I. Alexandrou, T.W. Clyne, G.A.J. Amaratunga, Chem. Phys. Lett. 373 (2003) 52–56.
[40] H. Kuzmany, R. Pfeiffer, M. Hulman, C. Kramberger, Philos. Trans. R. Soc. A Math. Phys. Eng. Sci. 362 (2004) 2375–2406.
[41] A.C. Ferrari, Solid State Commun. 143 (2007) 47–57.
[42] E. Cazzanelli, M. Castriota, L.S. Caputi, A. Cupolillo, C. Giallombardo, L. Papagno, Phys. Rev. B 75 (2007) 121405–121409.
[43] V. Scuderi, S. Scalese, S. Bagiante, G. Compagnini, L. D'Urso, V. Privitera, Carbon 47 (2009) 2134–2137.
[44] V.W. Brar, G.G. Samsonidze, M.S. Dresselhaus, G. Dresselhaus, R. Saito, A.K. Swan, M.S. Unlu, B.B. Goldberg, A.G. Souza, A. Jorio, Phys. Rev. B 66 (2002) 1594–1599.
[45] T. Bruno, A. Beretta, G. Groppi, M. Roderi, P. Forzatti, Catal. Today 99 (2005) 89–98.